ISSN:2790-1688 Volume-15-(2025)

Intelligent sensor-based multi-fault diagnosis of aero-engines using scattering characteristics

Junnan Cui [1], Muxuan Pan [1]

[1] College of Energy and Power Engineering, Nanjing University of Aeronautics and Astronautics, Nanjing,210006, China;

Abstract. To address the problem of insufficient real-time fault diagnosis accuracy in distributed intelligent sensors for aero-engine systems under multiple coexisting fault modes and limited computational resources, an intelligent sensor fault diagnosis method based on local data scattering feature optimization is proposed. First, a wavelet scattering network is employed to extract translation-invariant deep features from sensor signals, enabling efficient characterization of their time–frequency structures and energy distributions in resource-constrained environments. Subsequently, Principal Component Analysis (PCA) is applied to reduce the dimensionality of the high-dimensional scattering features, thereby removing redundant information and enhancing feature discriminability, which effectively improves diagnosis accuracy. Finally, a Support Vector Machine (SVM) multi-classification model is constructed based on the reduced features to achieve rapid fault-type identification, satisfying the real-time diagnostic requirements. Experimental results demonstrate that for typical sensor faults, including abrupt changes, drifts, offsets, and periodic disturbances, the proposed method achieves an average diagnosis accuracy of 98.2%, representing a 6.5% improvement compared with direct use of the original features. Moreover, the average diagnosis time per sample is only 32 ms, meeting the demands of high accuracy, low computational complexity, and real-time performance in aero-engine sensor applications.

Keywords: Aero-engine distributed control system; Wavelet scattering network; Time–frequency scattering features; Support vector machine; Principal component analysis.

1. Introduction

With the advancement of aero-engine technology, distributed control systems (DCS) have emerged as a key trend [1]-[3]. Intelligent sensors, as critical components of DCS, play a vital role in engine control and health management [4]-[5]. However, constrained by limited computational resources, intelligent sensors often struggle to achieve high accuracy and real-time performance in fault self-diagnosis. Thus, accurate and timely sensor fault diagnosis is essential to realizing distributed aero-engine control[6].

Existing sensor fault diagnosis methods fall into two categories: model-based and data-driven approaches[7]. Model-based methods require precise models and substantial computing power, which are often infeasible on resource-limited sensors. In contrast, data-driven methods align well with the real-time data acquisition capabilities of intelligent sensors. Nevertheless, conventional data-driven approaches often involve complex feature extraction or multi-sensor data fusion, which introduce high computational and communication costs, limiting their practicality.

To address these challenges, this paper proposes a lightweight and efficient fault diagnosis method using single-sensor data. A wavelet scattering network is first employed to extract high-dimensional, translation-invariant time–frequency features from raw signals[8]-[10]. With fixed parameters and low computational overhead, it is suitable for resource-constrained nodes[11]-[13]. Principal Component Analysis (PCA) is then applied to reduce feature dimensionality, retaining the most discriminative components while eliminating redundancy[15]. Finally, a Support Vector Machine (SVM) classifier is trained in the reduced subspace to achieve multi-fault recognition with a maximum-margin hyperplane.

The main contributions are as follows:(1) A lightweight diagnostic framework integrating wavelet scattering networks, PCA, and SVM is proposed. Compared to deep neural networks, it requires fewer computational resources and remains robust with small sample sizes.(2) PCA-based

feature reduction significantly decreases redundancy while preserving discriminative information, improving both accuracy and efficiency.(3) Experiments on aero-engine sensor data show that the method achieves over 98% diagnosis accuracy with millisecond-level latency, meeting the high-accuracy and low-latency requirements of aero-engine distributed control systems.

2. Extraction and Optimization of Scattering Features for Sensor Signals

2.1 Scattering Feature Extraction Based on Wavelet Scattering Network

The signals collected by aero-engine sensors are typical non-stationary signals. If Fourier transform is performed on them, time information will be lost. In contrast, wavelet transform can provide both time and frequency information of signals through the dilation and translation of wavelet functions, and it has multi-resolution characteristics, making it very suitable for time-frequency analysis of non-stationary signals.

On this basis, the wavelet scattering network draws on the structure of convolutional neural networks (CNNs). It performs convolution between the original signal and a preset wavelet filter, conducts modulus operation [16], and then performs local averaging via a low-pass filter. Finally, it obtains scattering features with invariance to translation and slight deformation. This calculation process can be systematically defined by a set of scattering paths (Scattering Paths).

Let the input signal be $f(t)$, where t is the time coordinate. Define $\Psi = \psi_j(t) j$ as a complex wavelet filter bank, where each wavelet $\psi_j(t)$ is generated by the scale parameter j ($j \in \mathbb{Z}^+$). $\psi_j(t)$ is a band-pass filter, and both its center frequency and bandwidth are proportional to 2^{-j}. This filter bank is used to extract multi-scale oscillatory information from the signal. Typically, this wavelet family is generated by scaling a mother wavelet, i.e., $\psi_j(t) = 2^{-j}\psi(2^{-j}t)$, and satisfies the admissible condition to ensure the invertibility of the transform.

Define a nonlinear operator $M : z(t) \to |z(t)|$, which takes the modulus of complex-valued signals and converts them into real-valued signals. This operation retains the signal envelope or amplitude information, removes high-frequency phase oscillations, and maintains translation equivariance.

Define a smoothing operation $A : z(t) \to z * \phi_J(t)$, where $\phi_J(t)$ is a low-pass scaling function with a support scale of 2^J, and J is the maximum scale parameter of the network, determining the degree of final invariance. This operation realizes local average pooling through convolution, providing translation invariance. The structure of the wavelet scattering network is shown in Fig. 1.

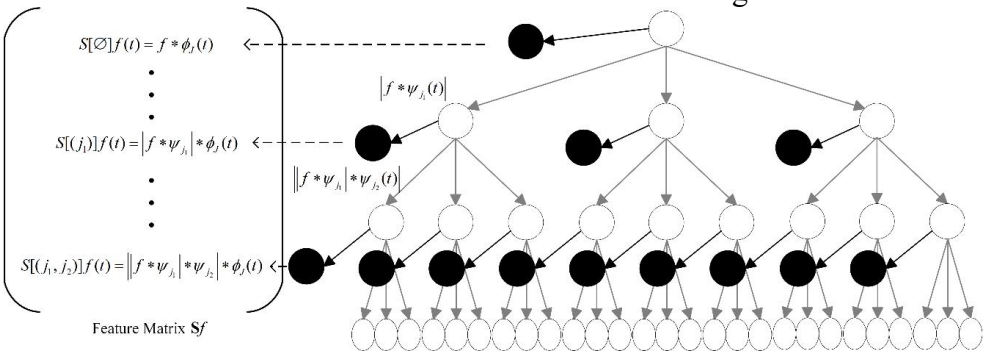

Fig. 1 Wavelet scattering network structure

The output of the network is a collection of coefficients calculated along all possible scattering paths $p = (j_1, j_2, ..., j_m)$. The path p defines a sequence of scales from which information is extracted, and its length m is referred to as the scattering order. The zeroth-order scattering coefficient is shown in Equation (1).

$$S[\varnothing]f(t) = f * \phi_J(t) \tag{1}$$

where $\varnothing$ denotes the empty path.

For the path $p=(j_1)$, the first-order scattering coefficient captures the average oscillatory energy of the signal at the scale 2^{j_1}. Its calculation is defined as:

$$U[j_1]f(t)=\left|f*\psi_{j_1}(t)\right| \tag{2}$$

$$S[(j_1)]f(t)=U[j_1]f*\phi_J(t)=\left|f*\psi_{j_1}\right|*\phi_J(t) \tag{3}$$

where $U[j_1]f(t)$ realizes band-pass filtering by convolving the input signal with a wavelet of scale j_1 to extract the complex-valued oscillatory component at this scale. $|\cdot|*\phi_J(t)$ performs low-pass filtering and local averaging on the amplitude signal, endowing it with translation invariance and outputting the final first-order scattering coefficient $S[(j_1)]f(t)$.

For the path $p=(j_1,j_2)$, its coefficient captures the "envelope of envelope" information (i.e., amplitude modulation structure) in the signal through two iterations. The calculation is defined as:

$$U[(j_1,j_2)]f(t)=\left|\left|f*\psi_{j_1}\right|*\psi_{j_2}(t)\right| \tag{4}$$

$$\begin{aligned}S[(j_1,j_2)]f(t)&=U[(j_1,j_2)]f*\phi_J(t)\\&=\left|\left|f*\psi_{j_1}\right|*\psi_{j_2}\right|*\phi_J(t)\end{aligned} \tag{5}$$

In the above formulas, the envelope of the first-order amplitude signal undergoes a second band-pass filtering $U[j_1]f*\psi_{j_2}(t)$ to analyze its own oscillatory mode at a finer scale j_2. If the envelope itself has changes (i.e., modulation), this operation will capture them. Then, the modulus is taken again to extract the envelope of the second oscillation, and then averaging is performed again to generate the stable second-order scattering coefficient $S[(j_1,j_2)]f(t)$.

The coefficients of the high-order path $p=(j_1,j_2,...,j_m)$ are defined recursively:

$$U[(j_1\quad j_k)]f(t)=\left|U[(j_1\quad,j_{k-1})]f*\psi_{j_k}(t)\right| \tag{6}$$

$$S[(j_1,...,j_m)]f(t)=U[p]f*\phi_J(t) \tag{7}$$

High-order coefficients characterize complex multi-modulation interactions in the signal. However, due to the energy compression property of the modulus operation (the energy of $||z|*\psi_j|$ is usually less than $|z|$), the energy of high-order coefficients decays rapidly. Therefore, in practical applications, it is usually sufficient to calculate up to the second order (m=2), i.e., $m\in 0,1,2$.

The output of the entire wavelet scattering transform $\mathbf{S}f$ is the set of scattering coefficients for all possible paths across all orders (from 0 to M):

$$\begin{aligned}\mathbf{S}f=\{&S[p]f(t):\text{for all paths}\,p=(j_1,\ldots,j_m)\\&\text{with}\,m\le M\ \text{and}\,j_1<j_2<\ldots<j_m\le J\}\end{aligned} \tag{8}$$

In practical applications, $S[p]f(t)$ is downsampled along the time axis to the Nyquist rate corresponding to the scale 2^J. Finally, $\mathbf{S}f$ can be organized into a feature matrix, serving as the input for the subsequent support vector machine (SVM) classifier.

2.2 Frequency-Domain Analysis of Fault Features in Sensor Signals

Sensor fault signals all have obvious separable feature differences in the frequency domain. For example, abrupt change faults usually cause transient high-frequency responses of signals, leading to concentrated energy bursts in the high-frequency band; while drift faults are mainly characterized by enhanced energy of low-frequency components in signals, which essentially result from the slow change of the signal baseline. In this paper, wavelet scattering transform is performed on normal sensor signals and signals of four typical fault types, and heatmaps of their first-order and second-order scattering coefficients are plotted, as shown in Fig. 2 and Fig. 3.

The horizontal axis of the heatmap represents time, the vertical axis represents the center frequency of the wavelet filter, and the color represents the energy magnitude of the scattering coefficient.

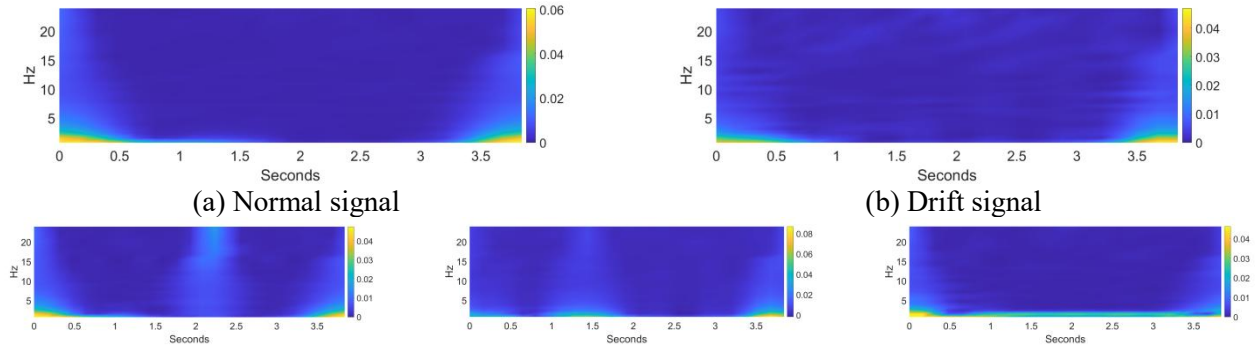

(a) Normal signal (b) Drift signal

(c) Spike signal (d) Bias signal (e) Periodic disturbance signal

Fig. 2 Heatmap of the first-order Scattering Coefficient of Sensor Signals

From the first-order scattering coefficient heatmap, it can be observed that compared with other signals, periodic disturbance signals exhibit a global high-energy distribution in the low-frequency band of 0–5 Hz. This phenomenon is consistent with the characteristic of periodic disturbances in the frequency domain, which are manifested as the superposition of the original signal and disturbances with a specific frequency.

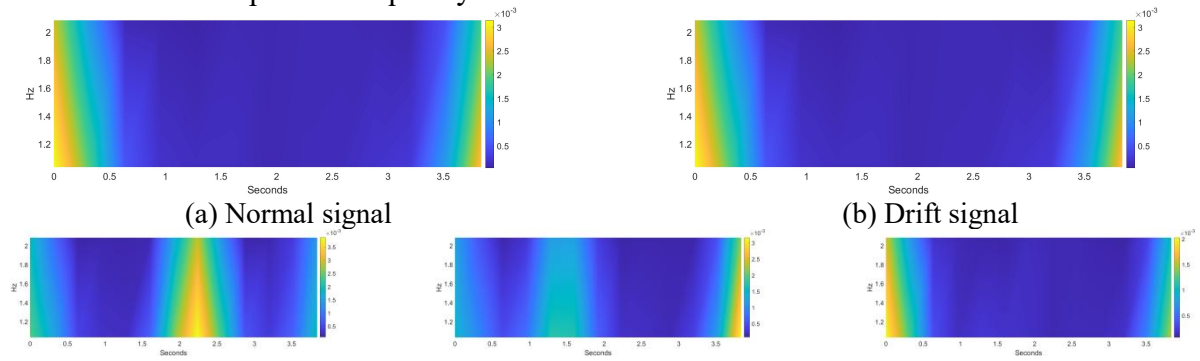

(a) Normal signal (b) Drift signal

(c) Spike signal (d) Bias signal (e) Periodic disturbance signal

Fig. 3 Heatmap of the second-order Scattering Coefficient of Sensor Signals

In the second-order scattering coefficient heatmap, the scattering coefficients of drift signals exhibit enhanced responses in the low-frequency filter bank and vary gently over time. Meanwhile, abrupt change signals show high-energy excitation in specific time periods. In contrast, offset signals are similar to abrupt change signals; however, since the offset persists after occurrence, they generate a relatively uniformly distributed energy frequency band.

2.3 Scattering Feature Optimization Based on PCA

Although scattering coefficients contain abundant energy distribution information and can provide effective representation for stable classification, they inherently have certain information redundancy [17]. This redundancy not only increases unnecessary computational burden and time complexity but also forces the Support Vector Machine (SVM) model to construct extremely complex hyperplanes to achieve class division. After converting the signal scattering feature matrix obtained in this paper into a vector, its dimension is usually greater than (note: the specific dimension value was not specified in the original text). At this point, the SVM can only select linear kernel functions suitable for high-dimensional inputs for mapping; meanwhile, limited by the insufficient number of samples, it fails to achieve good fault classification results. Therefore, it is necessary to perform dimensionality reduction and optimization on the obtained scattering coefficients.

This paper adopts Principal Component Analysis (PCA) to conduct dimensionality reduction on scattering features, and performs separability analysis on the scattering coefficients before and after dimensionality reduction. This analysis aims to verify the effectiveness of the proposed method in reducing feature redundancy, thereby making fault modes easier to be identified and classified by the SVM model. T-distributed Stochastic Neighbor Embedding (t-SNE) is a nonlinear dimensionality reduction visualization method [18], which can evaluate separability based on clustering performance. The evaluation results are shown in Fig. 4 and Fig. 5.

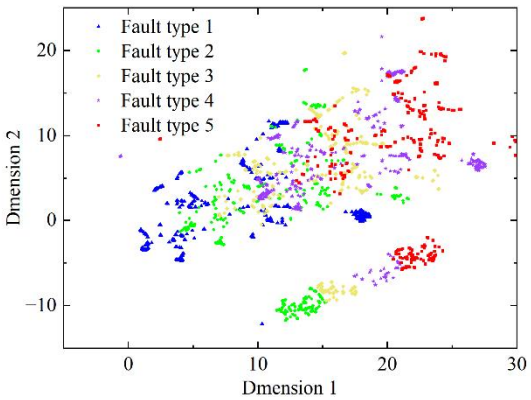

Fig. 4 t-SNE visualization of raw wavelet scattering features

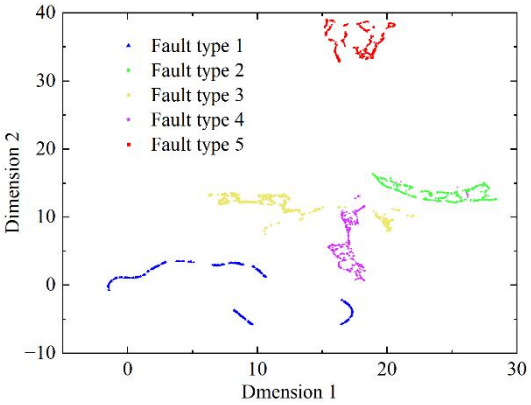

Fig. 5 t-SNE visualization of wavelet scattering features after PCA dimensionality

As shown in Fig. 2, the original wavelet scattering features contain substantial redundancy, leading to considerable overlap among different fault categories. Directly employing these high-dimensional features in an SVM model not only increases computational complexity but also limits diagnostic performance. In contrast, Fig. 3 demonstrates that after PCA-based dimensionality reduction, the scattering features exhibit improved inter-class separation in the feature space. This indicates that PCA effectively extracts the most discriminative low-dimensional components while eliminating redundant information. The enhanced compactness within classes and clearer boundaries between classes significantly facilitate the SVM in constructing a simpler yet effective hyperplane for accurate fault classification. Thus, PCA-optimized scattering features not only reduce computational cost but also establish a solid foundation for improved diagnostic performance.

3. Multi-Fault Diagnosis Method Based on Optimized Scattering Features

This paper proposes an intelligent fault diagnosis framework for sensors in aero-engine control systems, which is based on optimized scattering features and Support Vector Machine (SVM). This diagnosis framework is a systematic data processing and analysis process, mainly consisting of three core components: data acquisition, feature extraction, and fault mode classification, as shown in Fig. 6.

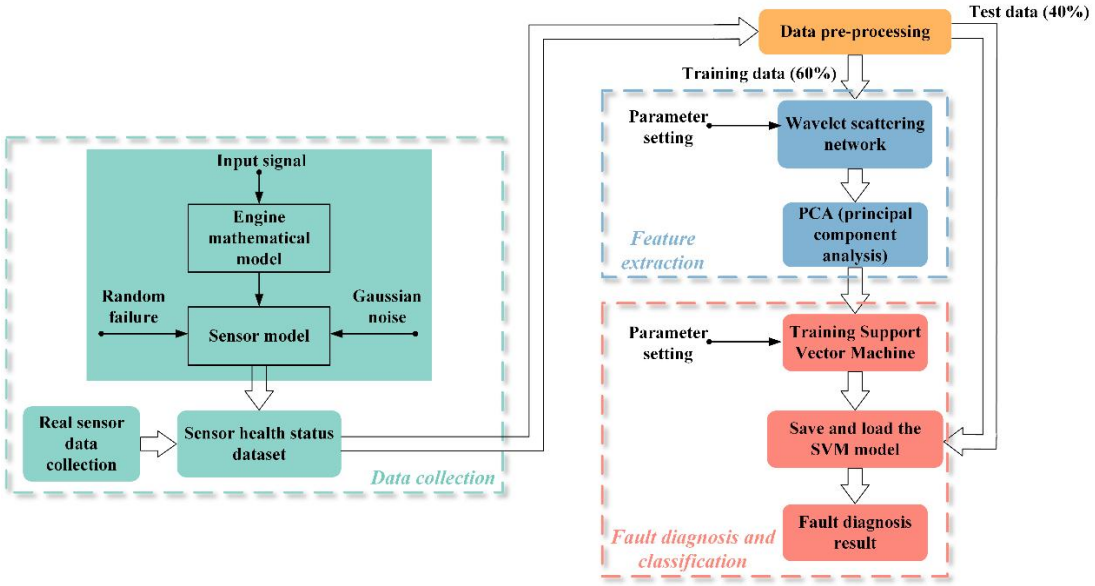

Fig. 6 Flowchart of Sensor Fault Diagnosis

Sensor models can usually be represented by a first-order or second-order inertial element. The sensor model adopted in this paper is a second-order inertial link with hysteresis, and its transfer function is given as follows:

$$G(s) = \frac{\omega_n^2}{s^2 + 2\xi\omega_n s + \omega_n^2} \cdot e^{-\tau s} \tag{9}$$

where $\omega_n = 9$, $\xi = 1.25$, $\tau = 0.12$.

The complete process of this method is as follows:

(1) Data Acquisition: Collect aero-engine sensor data under different operating conditions, and construct a comprehensive dataset covering normal status and multiple typical fault types.

(2) Signal Preprocessing: Perform systematic preprocessing operations on the original monitoring signals, including signal alignment and standardization, and set labels to lay a data foundation for subsequent feature extraction.

(3) Feature Extraction: Use a wavelet scattering network to extract deep signal features with translation invariance, and optimize and reduce the dimensionality of high-dimensional features through the Principal Component Analysis (PCA) algorithm to obtain low-dimensional feature representations with stronger discriminability.

(4) Fault Diagnosis and Classification: Based on the optimized feature vectors, construct a Support Vector Machine (SVM) multi-classification model to achieve accurate identification and classification of multiple sensor fault modes.

3.1 Scattering Feature Optimization Based on PCA

Signal preprocessing is a key step to ensure the reliability of sensor fault diagnosis [19]. Aiming at issues such as inconsistent dimensions and large differences in value ranges of original sensor signals, a data standardization method needs to be adopted for processing. This helps eliminate differences in feature scales and improve the performance and stability of subsequent feature extraction and classification models.

This paper adopts the Z-score standardization method, whose calculation formula is as follows:

$$x_{standardized} = \frac{x - \mu}{\sigma} \tag{10}$$

where μ represents the mean value of the signal, and σ represents the standard deviation of the signal.

3.2 Fault classification model based on support vector machine

Support Vector Machine (SVM), as a binary classification model based on statistical learning theory, is well-suited for sensor fault classification tasks involving small samples and nonlinear problems due to its structural risk minimization and strong generalization ability [14]. This paper extends its application to the problem of multi-fault diagnosis for sensors.

Given a training sample set $\{(\mathbf{v}_i, y_i) \mid i = 1, 2, \ldots, N\}$, where $\mathbf{v}_i \in \mathbb{R}^d$ is the optimized feature vector after PCA dimensionality reduction, and $y_i \in 1, 2, \ldots, K$ denotes the sensor fault category label. The core idea of SVM is to find an optimal hyperplane that maximizes the margin between samples of different classes. Its optimization problem is formulated as:

$$\min_{\mathbf{w},b} \ \frac{1}{2}\|\mathbf{w}\|^2 + C\sum_{i=1}^{N}\xi_i \tag{11}$$

$$\text{s.t.} \quad y_i(\mathbf{w}^T\kappa(\mathbf{v}_i) + b) \geq 1 - \xi_i \tag{12}$$

where $\mathbf{w}$ is the normal vector of the hyperplane; b is the bias term; $\kappa(\cdot)$ is the kernel function that maps data to a high-dimensional feature space; $C > 0$ is the penalty parameter, balancing the classification error and the margin size; and ξ_i is the slack variable, allowing a certain degree of classification error.

Considering the nonlinear characteristics of fault features, this paper adopts the Radial Basis Function (RBF) as the kernel function [19]:

$$K(\mathbf{v}_i, \mathbf{v}_j) = \exp(-\gamma \left\| \mathbf{v}_i - \mathbf{v}_j \right\|^2) \tag{13}$$

4. Experimental Verification and Result Analysis

4.1 Experimental Data and Experimental Setup

The experimental data used in this study consists of two parts: one part is the data actually collected by sensors during the operation of a certain type of aero-engine, and the other part is derived from simulations based on an aero-engine mathematical model.

The actually collected data is the data acquired by pressure sensors during the test run of a certain type of two-spool turbofan engine, and this data contains cases of abrupt change faults, as shown in Fig. 7.

This data is divided into 4-second segments, resulting in 350 segments in total. Among these segments, 16 contain abrupt change faults, which are labeled as abrupt change data.

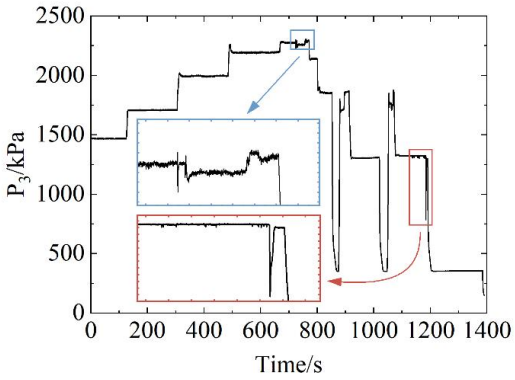

Fig. 7 Real sensor collected data

However, the actually collected data has a small number of samples and only contains one fault mode. Therefore, it is necessary to randomly inject faults into the output signals of the aero-engine mathematical simulation model to obtain a comprehensive training dataset. The training dataset includes the engine's dynamic acceleration process, dynamic deceleration process, and steady-state

process. The sampling frequency is 40 Hz, consistent with that of the actually collected data, and the acquisition period is 4 seconds.

The methods for simulating various faults are shown in Table 1. For example, periodic disturbance faults can be simulated by superimposing a periodic sine signal on the output signal of the engine mathematical model.

Table 1. Fault simulation method

Fault types	Simulation method
Drift signal	The original signal is shifted at a random rate
Bias signal	A small constant or random signal is superimposed on the original signal
Mutation signal	A pulse signal is superimposed on the original signal
Periodic disturbance signal	A signal of a certain frequency is superimposed on the original signal
Normal signal	No change

In addition, since faults are random in nature, this experiment obtains a large amount of fault data by adjusting parameters such as fault occurrence time, fault period, and fault amplitude during fault simulation. Considering the noise present in the actual sampling process of aero-engine sensors, Gaussian white noise is added during the acquisition process to enhance the authenticity of the simulated data. The time-domain diagrams of the sensor under 5 health conditions (including normal status and 4 fault types) in this paper are shown in Fig. 8.

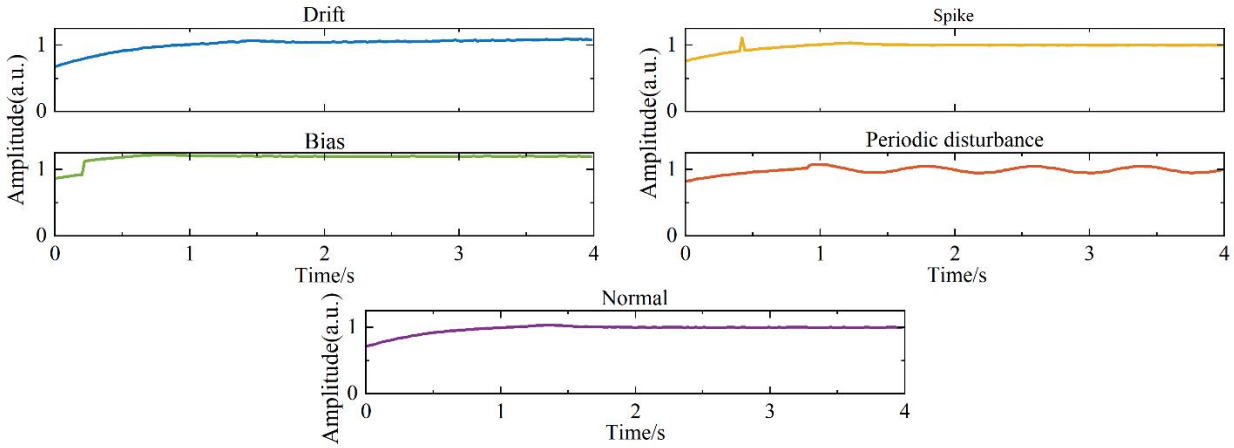

Fig. 8 Simulated sensor signals for 5 health conditions

Since deep learning-based diagnostic models rely on a large number of training samples, the scale of actually collected operational data is usually insufficient to meet this demand. On the other hand, certain specific fault modes are difficult to obtain or reproduce in real scenarios. Although simulated data cannot fully replicate all characteristics of real collected data, the fault features it reveals are highly similar to actual conditions and still have research value. Therefore, using simulated data to train the proposed diagnostic model is reasonable and necessary.

This study covers data on five sensor health states, with 500 data instances for each fault type, resulting in a total sample size of 2,500. To reduce the impact of random experimental fluctuations, all experiments were repeated 50 times and the average results were used.

The parameters of the wavelet scattering network are set as follows: the signal length is determined based on the actual length of the input data; the sampling frequency is 40 Hz; the scattering order is 2; the number of wavelet functions per octave (i.e., quality factor) in each layer is [8, 1]. After processing by the wavelet scattering network, the feature matrix of each sample has a dimension of 49×49, which is reduced to 7×7 via PCA. To verify the effectiveness of the optimized scattering features, the original scattering features were directly input into a Support Vector Machine (denoted as SVM2) for comparison with the proposed method (which uses the 7×7 dimensional PCA-reduced features as input, denoted as SVM1). Both models adopt the radial basis function kernel. Through 5-fold cross-validation, the parameters were determined: for SVM1, the kernel scale parameter γ_1 is 0.5 and the box constraint parameter C_1 is 10; for SVM2, γ_2 is 0.1

and C_2 is 20. Feature standardization is enabled for both models, and the classification covers the five target states involved in the experiment. The training set and test set of the two models are split at a 6:4 ratio, and the same data split is used to ensure fair comparison.

Based on the above setup, comparative tests were conducted on the two models. Indicators such as classification accuracy were used to verify the optimization effect of PCA dimensionality reduction on wavelet scattering features. The results show that the overall accuracy of SVM1 (based on reduced-dimensional features) is 98.2%, while that of SVM2 (based on original features) is 91.7%. The confusion matrices of their diagnostic results are shown in Fig. 9 and Fig. 10, respectively.

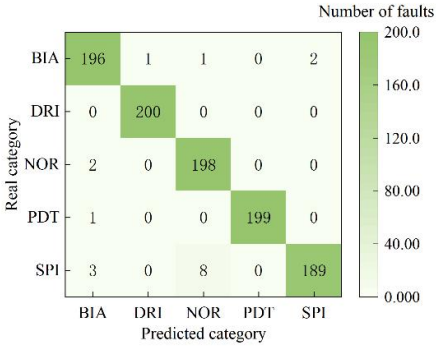

Fig. 9 Confusion matrix of SVM1 model

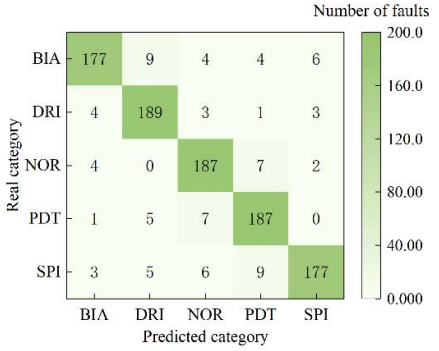

Fig. 10 Confusion matrix of SVM2 model

As can be seen from the figures, SVM1 (with PCA dimension-reduced features) has a high proportion of diagonal elements, few misclassifications, and clear decision boundaries. In contrast, SVM2 (with original features) has more and scattered misclassifications, and its decision surfaces are blurred due to high-dimensional redundancy. It is evident that PCA dimensionality reduction purifies features and significantly improves classification accuracy and robustness.

Furthermore, this study calculated three fine-grained metrics—Precision, Recall, and F1-Score—to comprehensively evaluate the performance balance of the models across different categories. The detailed results are shown in Table 2 and Table 3.

Table 2. Performance indicators of SVM1 model (PCA-reduced features)

Fault types	Precision	Recall	F1-Score
Drift signal	0.95652	0.99	0.97297
Bias signal	0.98953	0.945	0.96675
Spike signal	0.99502	1	0.99751
Periodic disturbance signal	0.9703	0.98	0.97512
Normal signal	1	0.995	0.99749
Macro indicator	0.98227	0.982	0.98197

Table 3. Performance indicators of the SVM2 model (without dimensionality reduction of features)

Fault types	Precision	Recall	F1-Score
Drift signal	0.90338	0.935	0.91892
Bias signal	0.94149	0.885	0.91237
Spike signal	0.90865	0.945	0.92647
Periodic disturbance signal	0.93651	0.885	0.91003
Normal signal	0.89904	0.935	0.91667
Macro indicator	0.9178	0.917	0.91689

When comparing the macro-average metrics of the two tables, the macro-average Precision, Recall, and F1-Score of SVM1 are all significantly higher than those of SVM2, and the fluctuation of each individual metric is smaller. This indicates that the dimension-reduced features not only improve the overall classification performance of the model but also make the recognition effect of each category more balanced, verifying the effectiveness of PCA feature optimization.

Based on the actual signal length and filter configuration, the total computation amount per sample of the algorithm proposed in this paper is approximately $7.98\times10^5\,FLOPs$, and its theoretical execution time on the ARM Cortex-A9 is about 0.32 ms.

This result indicates that the proposed algorithm only requires millisecond-level computation time on the embedded processor, which fully meets the requirements of real-time online diagnosis.

In summary, through the above series of experiments, the superiority of the algorithm proposed in this paper has been verified from three aspects: overall accuracy, detailed performance, and embedded performance prediction.

5. Summary

This paper investigates a lightweight fault diagnosis algorithm for intelligent sensors in distributed control systems of aero-engines, based on wavelet scattering networks, PCA dimensionality reduction, and a support vector machine classifier. The following conclusions are drawn:

(1) Wavelet scattering networks are employed to extract scattering features from sensor signals. These features effectively characterize the energy distribution of signals under different fault modes while retaining a certain degree of redundancy, thereby providing a foundation for subsequent feature optimization.

(2) Principal Component Analysis (PCA) is introduced to reduce the dimensionality of the scattering features, eliminating redundant information while retaining components with maximum variance and strong discriminative power. Consequently, the inter-class separation among different fault modes is significantly enhanced, and computational complexity is reduced.

(3) A multi-class Support Vector Machine (SVM) classification model is established based on the reduced-dimension features. By solving for hyperplanes between different classes of features, accurate diagnosis of multiple sensor faults is achieved. This method ensures a diagnostic accuracy higher than 98%, while maintaining millisecond-level latency per diagnosis, thereby meeting the high-accuracy and low-latency requirements for intelligent sensors in aero-engine distributed control systems.

References

[1] Jakovljevic M, Fulcher L, Benson D. Expectation and Vision for True modular Distributed Engine Control - Beyond 1st Project[C]//AIAA/ASME/SAE/ASEE Joint Propulsion Conference & Exhibit. Hartford, Massachusetts, USA, 2008.

[2] Thompson H A, Benitez-Perez H, Lee D, et al. A CANbus-based safety-critical distributed aeroengine control systems architecture demonstrator[J]. Microprocessors & Microsystems, 1999, 23(6): 345-355.

[3] Guo Y Q, Zhang H. Survey of the Distributed Control System for an Aeroengine[J]. Aeroengine, 2003, (03):52-55.

[4] Soussi A, Zero E, Sacile R, et al. Smart sensors and smart data for precision agriculture: a review[J]. Sensors, 2024, 24(8): 2647.

[5] SONG J Q, PAN M X, HUANG J Q. Technology analysis and system scheme for aero-engine distributed control system[J]. Journal of Aerospace Power, 2013, 28(10): 2391-2400.

[6] WU J J, ZHU X B, CHENG Y Q, et al. Research Progress of Intelligent Health Monitoring Technology for Liquid Rocket Engines[J]. Journal of Propulsion Technology, 2022, 43(1): 200668.

[7] CAO M, HUANG J Q, ZHOU J, et al. Current status, challenges and opportunities of civil aero-engine diagnostics & health management I: Diagnosis and prognosis of engine gas path, mechanical and FADEC[J]. Acta Aeronautica et Astronautica Sinica, 2022, 43(9): 625573.

[8] Liu C L, Hsaio W H, Tu Y C. Time series classification with multivariate convolutional neural network[J]. IEEE Transactions on Industrial Electronics, 2018, 66(6): 4788-4798.

[9] Hajihashemi V, Gharahbagh A A, Cruz P M, et al. Binaural Acoustic Scene Classification Using Wavelet Scattering, Parallel Ensemble Classifiers and Nonlinear Fusion[J]. Sensors. 2022, 22, 1535.

[10] LUO D S, WANG Y K, WANG C M. Fault diagnosis of rolling bearing based on time-frequency graph and convolutional neural network[J]. Control Engineering of China, 2024. DOI:10.14107/j.cnki.kzgc.20240405.

[11] Mallat S. Understanding deep convolutional networks[J]. Philosophical Transactions of the Royal Society A: Mathematical, Physical and Engineering Sciences, 2016, 374(2065): 20150203.

[12] Mallat S. Group invariant scattering[J]. Communications on Pure and Applied Mathematics, 2012, 65(10): 1331-1398.

[13] Bruna J, Mallat S. Invariant scattering convolution networks[J]. IEEE Transactions on Pattern Analysis and Machine Intelligence, 2013, 35(8): 1872-1886.

[14] XIE Z D, TAN X, YUAN X W, et al. Small sample signal modulation recognition algorithm based on support vector machine enhanced by generative adversarial networks generated data[J]. Journal of Electronics and Information Technology, 2023, 45(6): 2071-2080.

[15] Jolliffe I T, Cadima J. Principal component analysis: a review and recent developments[J]. Philosophical Transactions of the Royal Society A, 2016, 374(2065): 20150202.

[16] Wiatowski T, Bolcskei H. A mathematical theory of deep convolutional neural networks for feature extraction[J]. IEEE Transactions on Information Theory, 2018, 64(3): 1845-1866.

[17] Liu L, Wu J, Li D, et al. H. Fractional wavelet scattering network and applications[J]. IEEE Transactions on Biomedical Engineering, 2019, 66(2): 553563.

[18] Zhang S Q, Duan X N, Zhang L G, et al. Tsne dimension reduction visualization analysis and moth flame optimized ELM algorithm applied in power load forecasting[J]. Proceedings of the CSEE, 2021, 41(9): 3120–3129.

[19] Ding S F, Qi B J, Tan H Y. An overview on theory and algorithm of support vector machines[J]. Journal of University of Electronic Science and Technology of China, 2011, 40(1): 2–10.